

## Cyclorotation Models for Eyes and Cameras

Miles Hansard, Radu Horaud

► **To cite this version:**

Miles Hansard, Radu Horaud. Cyclorotation Models for Eyes and Cameras. IEEE Transactions on Systems, Man, and Cybernetics, Part B: Cybernetics, Institute of Electrical and Electronics Engineers, 2010, 40 (1), pp.151-161. <[http://ieeexplore.ieee.org/xpls/abs\\_all.jsp?arnumber=5109657](http://ieeexplore.ieee.org/xpls/abs_all.jsp?arnumber=5109657)>. <10.1109/TSMCB.2009.2024211>. <inria-00435549>

**HAL Id: inria-00435549**

**<https://hal.inria.fr/inria-00435549>**

Submitted on 24 Nov 2009

**HAL** is a multi-disciplinary open access archive for the deposit and dissemination of scientific research documents, whether they are published or not. The documents may come from teaching and research institutions in France or abroad, or from public or private research centers.

L'archive ouverte pluridisciplinaire **HAL**, est destinée au dépôt et à la diffusion de documents scientifiques de niveau recherche, publiés ou non, émanant des établissements d'enseignement et de recherche français ou étrangers, des laboratoires publics ou privés.

# Cyclo-rotation Models for Eyes and Cameras

Miles Hansard and Radu Horaud

**Abstract**—The human visual system obeys Listing’s law, which means that the cyclo-rotation of the eye (around the line of sight) can be predicted from the direction of the fixation point. It is shown here that Listing’s law can be conveniently formulated in terms of rotation matrices. The function that defines the observed cyclo-rotation is derived in this representation. Two polynomial approximations of the function are developed, and the accuracy of each model is evaluated by numerical integration over a range of gaze directions. The error of the most simple approximation, for typical eye movements, is less than half a degree. It is shown that, given a set of calibrated images, the effect of Listing’s law can be simulated in a way that is physically consistent with the original camera. This is important for robotic models of human vision, which typically do not reproduce the mechanics of the oculomotor system.

**Index Terms**—Biological control systems, visual system, robot kinematics.

## I. INTRODUCTION

This paper explores a kinematic property of human eye-movements, using geometric and numerical methods. The objective is to model the rotation of the human eye in terms of the standard camera model from computer vision [1]. This work is motivated by the need to use real image-data in computational models of human vision. It will be shown, in particular, that the images obtained from a standard robotic camera-mounting can be made compatible with the observed orientations of the human eye. This means that subsequent geometric analysis of the images will be consistent with the behaviour of the oculomotor system. The results described here provide a foundation for the further development of both monocular and binocular models of biological vision [2]–[4].

### A. Visual Orientation

There are several types of human eye-movement, including those that are used to stabilize the retinal image during motion of the head, and those that are specific to binocular vision [5]. This work, however, is chiefly concerned with *saccadic* eye movements, which are used to fixate visual targets in the scene.

The fixation of a target-point defines the *direction* but not the complete *orientation* of the eye. This is because the orientation includes the ‘cyclo-rotation’, around the ray that joins the optical centre<sup>1</sup> to the target, as well as the direction. In geometric terms, the direction can be specified by a suitable choice of two spherical angles, such as elevation and azimuth. The orientation involves a third angle, which accounts for the cyclo-rotation, or ‘torsion’ around the line of sight. Listing’s

law, as will be explained, describes the observed relationship between visual direction and orientation.

The complete orientation of the eye can be consistently determined from the gaze direction, as follows. Suppose that the visual target is represented, with respect to a reference direction, by elevation and azimuth angles  $\alpha$  and  $\beta$ . Then the cyclo-rotation  $\gamma$  can be treated as a function  $\gamma(\alpha, \beta)$ . This is the principle of *Donders’ law* [5], [6], which states that the actual torsion of the eye is determined by the gaze direction, so that the final orientation is fully determined by the visual target. Note however, that Donders’ law does not actually *define* the function  $\gamma(\alpha, \beta)$ .

### B. Ocular Kinematics

Donders’ law asserts that torsion is consistently determined by the oculomotor system, but does not make any further predictions. A more specific model can be formulated by noting that, given an initial orientation, the subsequent angles and axes of rotation can be used to predict the final torsion.

Hence the actual cyclo-rotation function  $\gamma(\alpha, \beta)$  can be derived from a geometric model of visual orientation. This is the principle of Listing’s law, which quantifies Donders’ law in the following way: *There exists a unique reference orientation, such that any other observed orientation of the eye can be obtained by a single rotation, around an axis perpendicular to the reference direction* [5], [6]. It follows that, although the axis of rotation depends on the target direction, it must lie in *Listing’s plane*, which is itself perpendicular to the reference direction. The unique reference orientation of the eye is called *primary position*. The reference direction, which is determined by experiment, is approximately straight-ahead. It follows that Listing’s plane is approximately parallel to the face [7]. Note that Listing’s law does not determine the rotational *movement* of the eye; rather, it states that the observed torsion is compatible with a particular choice of rotation.

Listing’s law is applicable if the head is upright and static, and if the fixation point is distant. The torsion, in these conditions, can be predicted with an accuracy of around one degree [5], [7]. Listing’s law can be extended to describe the case in which the eye moves from a general (i.e. non-primary) position. The rotation axes remain co-planar in this case, but the plane is no longer orthogonal to the initial direction [6], [8]. Most of the relevant experimental literature is concerned with primate vision, although support for Listing’s law has also been found in other species, including Chameleons [9].

Donders’ law can be justified with respect to the kinematics of the eye: Cyclo-rotation is not a component of visual direction, and so the oculomotor control problem can be simplified by removing this degree of freedom. Experimental evidence

From: INRIA Rhône-Alpes, 655 Avenue de l’Europe, 38330 Montbonnot, France. This work is part of the *Perception on Purpose* project, supported by EU grant 027268.

<sup>1</sup>It will be assumed that the eye has a fixed centre of rotation, and that this point coincides with the optical centre [5].

suggests that the human eye is not mechanically constrained to behave in this way. For example, irregular torsion is observed in eye movements that occur during sleep [10]. The particular form of Listing’s law has been justified with respect to both ‘motor’ and ‘visual’ criteria. For example, it has been shown that the law is related to the minimization of muscular effort, of total cyclo-rotation, and of binocular disparity [4], [6], [11].

It is useful, as explained above, to think of Donders’ law as a rule  $\gamma(\alpha, \beta)$  that associates a cyclo-rotation angle  $\gamma$  with each visual direction  $(\alpha, \beta)$ , such that the complete orientation of the eye is given by the three angles  $\alpha$ ,  $\beta$  and  $\gamma(\alpha, \beta)$ . In order to derive the form of this function from Listing’s law, it is first necessary to define the parameterization of visual direction. Here the angles  $\alpha$  and  $\beta$  will be assigned to the elevation and azimuth of the target, respectively. This is the ‘Helmholtz’ coordinate system [4], [6], [12]–[14], in which the visual direction swings in a plane containing the inter-ocular axis; the plane itself rotates *around* the inter-ocular axis, as shown in figure 1.

This azimuth-elevation scheme is the natural choice, for four related reasons. Firstly, it means that torsion can be measured with respect to a reference plane, defined by the two optical centres and the fixation point, which is intrinsic to the viewing configuration. There is no need for an external definition of ‘horizontal’ and ‘vertical’. Secondly, the elevation of any visual direction can be adjusted without affecting the azimuth. This is desirable with respect to the measurement of eye-movements, because the straight-ahead azimuth is easily defined (by making the visual direction orthogonal to the inter-ocular axis), whereas the straight-ahead elevation is more difficult to determine [5]. Thirdly, the geometry of binocular vision can be more readily described in Helmholtz coordinates, because each elevation plane contains corresponding epipolar lines in the left and right images [15]. Fourthly, the definition of  $\gamma(\alpha, \beta)$  is simple and symmetric in the Helmholtz coordinate system (see section VI). The alternative definition in ‘Fick’ coordinates [5], [16], where  $\alpha$  and  $\beta$  are longitude and latitude, is less concise.

### C. Robotic Systems

The Helmholtz scheme is also the natural configuration for an active binocular robot-head [17], [18]. This is because the left and right pan-motors can be fixed parallel to each other, such that the visual axes are co-planar. It follows that, as the cameras converge, the axes will (ideally) intersect in space. Hence binocular fixation can be mechanically approximated. This type of robot does not obey Listing’s law, as will be shown in section V. However, in order to simulate human vision with such a system, the method of section IX can be used to appropriately cyclo-rotate the original images. The present work, for the purpose of simulating human vision, provides an alternative to the mechanical implementation of Listing’s law [19], [20]. Robot-heads of the latter type are, in comparison with the Helmholtz configuration, more difficult to construct and control [17].

### D. Gaze Tracking

Listing’s law is also relevant to the design of gaze-tracking systems [21], [22]. For example, greater accuracy can be achieved by accounting for the small angular difference between the line-of-sight (defined in relation to the fovea) and the optical axis of the eye [5], [23]. If the latter can be estimated, then the plane containing the two rays can be obtained from Listing’s law. The line-of-sight is at a fixed angular offset, in this plane, from the optical axis [24]. Listing’s law can also be used to relate the direction of gaze to the projection of the iris, in a calibrated video of the eye [25].

### E. Geometric Models

The mathematical expression of Listing’s law depends on the representation of the relevant eye-movements. The three-dimensional rotation group can be parameterized in several different ways [26]. The quaternion [8], [12], [14], rotation vector [27], [28] and geometric algebra [29] parameterizations, which are closely related, are particularly well-suited to the modelling of ocular kinematics. It is also possible to represent a rotation by a pair of reflections, leading to a more geometric interpretation of Listing’s law [30]. The present work emphasizes the computational aspects of Listing’s law, which is formulated here in terms of rotation matrices. The matrix representation has the advantages of being both mathematically familiar, and computationally convenient. Furthermore, it can immediately be combined with standard projection-models from the computer vision literature. This is useful for geometric analysis of the retinal image, in relation to Listing’s law, as described in section IX.

### F. Novel Contributions

This work describes new results in the representation, approximation and simulation of Listing’s law. Primarily, a new derivation of the torsion function  $\gamma(\alpha, \beta)$  is made in sections IV–VI. There are two objectives here. Firstly, Listing’s law will be expressed in terms of rotation matrices, so that it can readily be incorporated into the standard camera model of computer vision [1]. Secondly, these rotation matrices will be suitable for the analysis of binocular vision. This means that the results obtained here provide a foundation for further analyses of binocular kinematics [2].

Two approximations (one of which has been used previously, e.g. [4]) of the Listing cyclo-rotation are made in section VII. The advantage of these approximations is that they dispense with the trigonometric functions in the exact formula. This makes it easier to incorporate cyclo-rotation into theoretical models of oculomotor control [3], [4]. The results described above are visualized by stereographic projection. The objective of the visualization is to understand the pattern of cyclo-rotation across the visual field.

A procedure for the numerical integration of ocular torsion is introduced in section VIII, where it is used to estimate the accuracy of the approximate cyclo-rotation models described above. This numerical evaluation is complementary to the analytic approach that has been taken elsewhere [11]. The

objective is establish the range of visual directions over which the approximate models can be used. This evaluation also justifies the approximations that have been used in previous work (e.g. [3], [4]).

Finally, in section IX, an algorithm for the simulation of Listing's law is presented. The proper way to simulate ocular torsion, given a set of calibrated images, has not been addressed previously. Here the objective is to understand how the cyclo-rotation relates to the extrinsic and intrinsic parameters of the camera [1].

### G. Organization of the Paper

The body of the present work is organized as follows. section II introduces the necessary notation, and defines the primary position of the eye. A useful visualization procedure, based on stereographic projection, is described in section III. Matrix representations of Listing and Helmholtz orientation are developed in sections IV and V, respectively. The Listing cyclo-rotation is derived in section VI. Approximations of the cyclo-rotation are developed in section VII. The accuracy of each approximation is evaluated in section VIII. It is shown in section IX that, given a set of images, the preceding results can be used to simulate the effects of ocular torsion. section X contains the conclusion of the paper.

## II. SCENE COORDINATES

Each scene-point  $\mathbf{p} = (x, y, z)^\top$  is represented in a head-fixed coordinate system, as illustrated in figure 1. The origin is located at the rotational centre of the left eye,  $\mathbf{e} = (0, 0, 0)^\top$ , which is assumed to coincide with the optical centre [5]. The axes of the coordinate system are  $\{\mathbf{x}, \mathbf{y}, \mathbf{z}\}$ , with  $\mathbf{x}$  and  $\mathbf{y}$  parallel to the coronal ('face') plane. The vector  $\mathbf{x}$  points rightwards along the inter-ocular axis (from the subject's point of view), while  $\mathbf{y}$  points downwards. The coordinate system is right-handed, and so it follows that  $\mathbf{z}$  is perpendicular to the coronal plane, and points out into the scene. It will be assumed that, when the eye is in primary position,  $\mathbf{z}$  is aligned with the visual axis. The plane that is perpendicular to  $\mathbf{x}$  intersects the eyeball in a great circle which, in primary position, defines the *vertical meridian* of the eye. The plane that is perpendicular to the  $\mathbf{y}$  axis defines, in primary position, the *horizontal meridian* of the eye. It will be assumed that these meridians are fixed on the eye (not in the head).

The target point is  $\mathbf{p}$ , which lies in a visual direction represented by the unit-vector

$$\mathbf{v} = \mathbf{p}/d, \quad (1)$$

where  $d = |\mathbf{p}|$  is the Euclidean distance to  $\mathbf{p}$ . The target-point is fixated by a rotation of the primary line of sight,  $\mathbf{z}$ , onto the target direction,  $\mathbf{v}$ . This will be expressed as

$$\mathbf{R}\mathbf{z} = \mathbf{v} \quad (2)$$

where  $\mathbf{R}$  is a  $3 \times 3$  rotation matrix. If the target point lies in either the horizontal plane  $\{\mathbf{x}, \mathbf{z}\}$ , or in the vertical plane  $\{\mathbf{y}, \mathbf{z}\}$ , then the eye is in a *secondary position* after the rotation. The fixation of a generic scene point leaves the eye in a *tertiary position* [5].

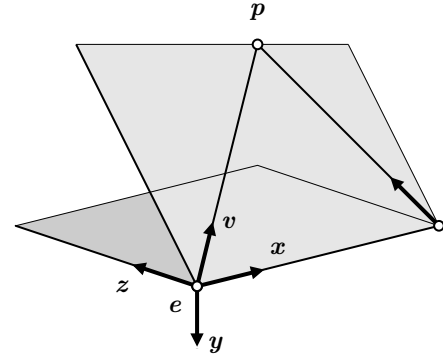


Fig. 1. The two eyes fixate a point  $\mathbf{p}$  in the scene, which is shown here from the back-left. The rotation of one eye (here the left), with optical centre  $\mathbf{e}$ , will be analyzed with respect to the coordinate system  $\{\mathbf{x}, \mathbf{y}, \mathbf{z}\}$ . The vectors  $\mathbf{x}$  and  $\mathbf{z}$  correspond to the inter-ocular and straight-ahead directions, respectively. The vector  $\mathbf{v}$  corresponds to the visual direction of  $\mathbf{p}$  from the left optical centre  $\mathbf{e}$ . Note that the left and right visual directions lie in a common epipolar plane.

It will be assumed, in the following sections, that the eye begins in primary position  $\mathbf{z}$ , and rotates to fixate the target point  $\mathbf{p}$ . If the eye begins in a non-primary position, then it can be shown that Listing's plane is rotated in space, by half the angle of the initial direction [7], [30]. This case will not be analyzed here.

Several different coordinate conventions have been used in the literature (e.g. [6], [8], [12]). The system described above was chosen for two reasons. Firstly it is consistent with the computer-vision literature, in which  $\mathbf{z}$  is usually the optical axis. Secondly, it is convenient in the binocular case, which emphasizes the family of planes containing the inter-ocular axis. Here the convention of  $\mathbf{x}$  pointing rightwards is kept for these planes.

## III. STEREOGRAPHIC PROJECTION

The orientation of the eye is visualized, in the present work, by stereographic projection [5], [6]. This procedure, which is illustrated in figure 2, is defined as follows. The eyeball is represented by the unit sphere  $\mathcal{S}$ , located at  $\mathbf{e}$ . The stereographic centre of projection  $\mathbf{s}_0 = (0, 0, -1)^\top$  is fixed in the head, at the back of of the eyeball. A projection plane  $\mathcal{T}$  is fixed in space, perpendicular to the  $\mathbf{z}$  axis. Now consider a landmark on the eyeball, with coordinates  $(v_x, v_y, v_z)^\top$ ; this point, together with  $\mathbf{s}_0$ , defines a ray. The intersection of the ray with the plane  $\mathcal{T}$  defines the stereographic projection  $(\xi, \eta)$  of the landmark. For example, if  $\mathcal{T}$  passes through the centre of  $\mathcal{S}$ , then the projection is

$$(\xi, \eta) = \frac{(v_x, v_y)}{1 + v_z}. \quad (3)$$

Any point, other than  $\mathbf{s}_0$ , can be mapped to the plane in this way. In particular, the entire forward-hemisphere of visual directions  $\{\mathbf{v} : |\mathbf{v}| = 1, v_z \geq 0\}$  is mapped to the unit disc, centred at  $(0, 0)^\top$  in  $\mathcal{T}$ .

The orientation of the eye will be visualized by projecting a notional cross, which is marked on the cornea of the eye, and aligned with the pair planes that contain the horizontal and vertical retinal meridians. If the eye rotates to fixate a point

$p$ , then the cross will take coordinates  $(v_x, v_y, v_z)^\top$ , which can be projected to  $(\xi, \eta)$  via equation (3). The procedure is illustrated in fig. 2 where, for clarity, the plane  $\mathcal{T}$  is shown *in front* of the eyeball (the principle is the same).

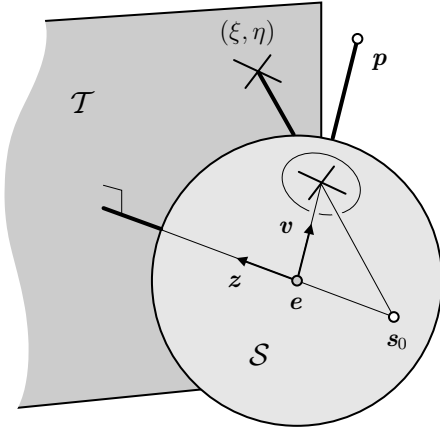


Fig. 2. Stereographic Projection. A schematic diagram of the procedure used to construct figures 4, 5, 7 and 8. The eyeball, which is centred on the point  $e$ , is seen from the back-left, as in fig. 1. The stereographic plane  $\mathcal{T}$  is perpendicular to the head-fixed  $z$ -axis. The eye is fixating a scene-point  $p$ ; the corresponding vector,  $v$ , points *into* the page. A reference cross, which is fixed to the cornea, is projected onto  $\mathcal{T}$ . The centre of projection,  $s_0$ , is fixed in the head, at the back of the eye.

The stereographic projection preserves several properties of the underlying rotation group [26]. This means that the procedure gives an effective visualization of ocular orientation, as can be seen in figures 4 and 5. For example, consider the ‘spokes’ of parallel crosses that appear in figure 5a; these correspond to *geodesic paths* through the space of orientations. The eye moves directly from the central point, with no additional rotation of the cross.

It should be emphasized that, in the present work, stereographic projection is used only for visualization. It is *not* used to describe the retinal projection of the scene. Indeed, the stereographic and optical centres of projection,  $s_0$  and  $e$  respectively, are quite distinct (see fig. 2).

#### IV. LISTING ORIENTATION

Listing’s law states that the actual orientation of the eye, as  $p$  is fixated, is consistent with a rotation of the primary line of sight  $z = (0, 0, 1)^\top$  around a perpendicular axis  $w$ . It follows that, for any target  $p$ , the corresponding axis  $w$  is in the plane  $\{x, y\}$ ; this, in the present context, is Listing’s plane. The axis is defined as

$$w = z \times v \quad (4)$$

$$= \sin(\phi) (\sin \theta, \cos \theta, 0)^\top \quad (5)$$

where  $\phi$  is the angle of rotation (from  $z$  to  $v$ ), and  $\theta$  is the direction of the axis in the  $\{x, y\}$  plane, as shown in figure 3. The angle  $\theta$  is in the range  $0 \leq \theta < 2\pi$ ; in particular, if  $\theta = 0$ , then  $w$  is parallel to  $y$ , and the rotated line of sight lies in the  $\{x, z\}$  plane. The angle  $\phi$  can be unambiguously recovered from

$$\sin \phi = \sqrt{w \cdot w}, \quad (6)$$

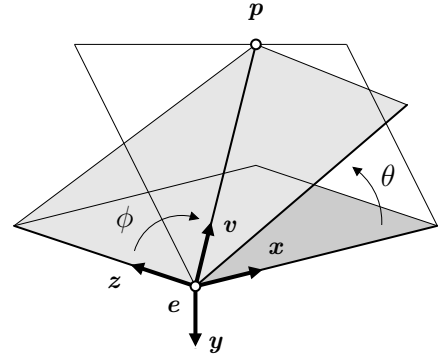


Fig. 3. Listing Coordinates (c.f. fig. 6). The optical centre of the eye is located at point  $e = (0, 0, 0)^\top$ . The initial gaze direction, with the eye in ‘primary position’, is along the  $z$  axis. In order to fixate the point  $p$ , a rotation through angle  $\phi$  is required. The axis  $w$  of the rotation is *perpendicular* to the  $\{z, v\}$  plane, and *in* the  $\{x, y\}$  plane. The axis is inclined from the vertical by an angle  $\theta$ .

because of the physical constraint  $0 \leq \phi \leq \pi/2$ .

The axis  $w$  and angle  $\phi$  define the Listing rotation, which will be represented by a  $3 \times 3$  matrix  $R_L$ . Rodrigues’ equation [26] is used to compute  $R_L$  from  $w$  and  $\phi$ ; this results in

$$R_L = (x_L, y_L, z_L) = \begin{pmatrix} 1 - \lambda \cos^2 \theta & \lambda \cos \theta \sin \theta & \cos \theta \sin \phi \\ \lambda \cos \theta \sin \theta & 1 - \lambda \sin^2 \theta & -\sin \theta \sin \phi \\ -\cos \theta \sin \phi & \sin \theta \sin \phi & \cos \phi \end{pmatrix} \quad (7)$$

where  $x_L$ ,  $y_L$  and  $z_L$  are the columns of the matrix, and the versine

$$\lambda = 1 - z \cdot v \quad (8)$$

$$= 1 - \cos \phi \quad (9)$$

has been introduced for notational convenience. The vector  $z_L$  is the rotated line of sight,  $R_L z$ , while  $\{x_L, y_L\}$  are the rotated retinal axes. Equation (7) is a mathematical expression of Listing’s law (cf. sec. I-B).

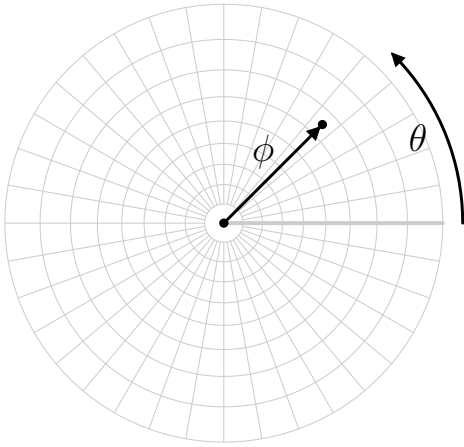
The stereographic coordinates of the Listing rotation are shown in figure 4a, where the concentric circles are parameterized by  $\theta$ , and the radial spokes are parameterized by  $\phi$ . The ocular orientations that result from Listing’s law are illustrated in figure 5a. Note that the crosses, each of which encodes the ocular torsion, are parallel in this representation.

#### V. HELMHOLTZ ORIENTATION

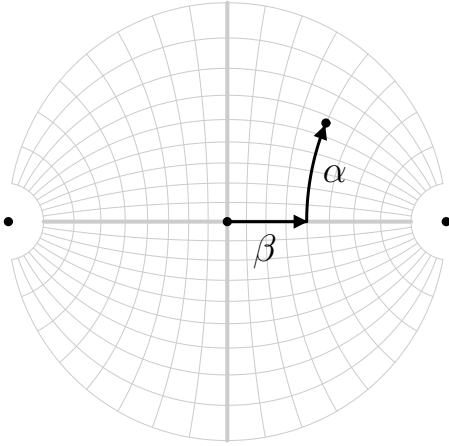
It was shown, in the preceding section, that the target visual direction  $v$  can be reached by a rotation  $R_L$  of  $z$ , around a variable axis  $w$ . In order to quantify the torsion that is associated with this rotation, it will be necessary to establish a reference-system of rotations. These will be defined with respect to the fixed axes  $\{x, y, z\}$ . It is, as described in the introduction, convenient to use the *Helmholtz* rotation,

$$R_H = AB \quad (10)$$

where  $A$  represents a rotation around  $x$ , and  $B$  represents a rotation around  $y$ . The two factors are defined as follows. The



(a) Stereographic projection of the Listing coordinate system  $(\theta, \phi)$ , cf. fig. 3. The primary direction is mapped to the centre of the disc; the boundary represents targets at  $\phi = 90^\circ$  eccentricity.



(b) Stereographic projection of the Helmholtz coordinate system  $(\alpha, \beta)$ , cf. fig. 6. The points on the far left and right represent the intersection of the inter-ocular axis with the eyeball.

Fig. 4. Figures 4a and 4b show the stereographic projection of the Listing and Helmholtz coordinate systems, respectively. The track from the origin shows the path of the visual axis as the eye turns to fixate in the direction  $\theta = 45^\circ$ ,  $\phi = 65^\circ$ . Note that this involves one rotation in 4a, and two rotations in 4b. A spacing of  $10^\circ$  is used for each family of coordinate lines.

rotation matrix

$$\mathbf{A} = \begin{pmatrix} 1 & 0 & 0 \\ 0 & \cos \alpha & -\sin \alpha \\ 0 & \sin \alpha & \cos \alpha \end{pmatrix} \quad (11)$$

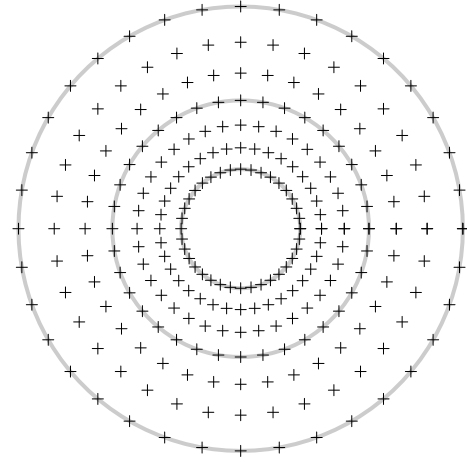
is associated with the *elevation* angle  $\alpha$  of the target, and the rotation matrix

$$\mathbf{B} = \begin{pmatrix} \cos \beta & 0 & \sin \beta \\ 0 & 1 & 0 \\ -\sin \beta & 0 & \cos \beta \end{pmatrix} \quad (12)$$

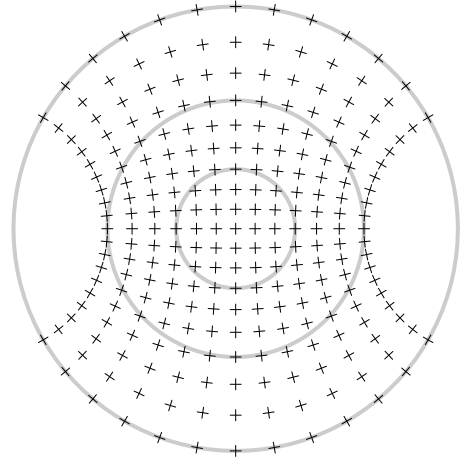
is associated with the *azimuth* angle  $\beta$  of the target. The azimuth and elevation are defined as

$$\tan \alpha = -v_y/v_z \quad (13)$$

$$\sin \beta = v_x/d \quad (14)$$



(a) Listing Orientations, plotted in  $(\theta, \phi)$  coordinates, cf. figure 4a.



(b) Helmholtz Orientations, plotted in  $(\alpha, \beta)$  coordinates, cf. figure 4b.

Fig. 5. (a) Stereographic projection of Listing orientations, plotted in polar coordinates  $(\theta, \phi)$ . Note that the retinal orientations are mutually parallel in this representation. Solid circles indicate eccentricities of  $30^\circ$ ,  $60^\circ$  and  $90^\circ$ . Some crosses are omitted in the central region, for clarity. (b) Helmholtz orientations, plotted in  $(\alpha, \beta)$  coordinates. Note that the retinal orientations are *not* mutually parallel in this representation. The horizontal meridian of each possible orientation lies in an azimuthal plane.

where  $d$  is the distance to the target, as in (1). Note that points with positive elevation are above the optical centre ( $y < 0$ ), while points with positive azimuth are to the right of the optical centre ( $x > 0$ ). The angular ranges are  $-\pi/2 \leq \alpha \leq \pi/2$  and  $-\pi/2 \leq \beta \leq \pi/2$ . The Helmholtz rotation is illustrated in figure 6.

The explicit form of the Helmholtz matrix  $\mathbf{R}_H$  is obtained by substituting (11) and (12) into (10), and performing the multiplication; this results in

$$\mathbf{R}_H = (\mathbf{x}_H, \mathbf{y}_H, \mathbf{z}_H) = \begin{pmatrix} \cos \beta & 0 & \sin \beta \\ \sin \alpha \sin \beta & \cos \alpha & -\sin \alpha \cos \beta \\ -\cos \alpha \sin \beta & \sin \alpha & \cos \alpha \cos \beta \end{pmatrix} \quad (15)$$

Note that, by analogy with (7),  $\mathbf{z}_H$  is the rotated line of sight,

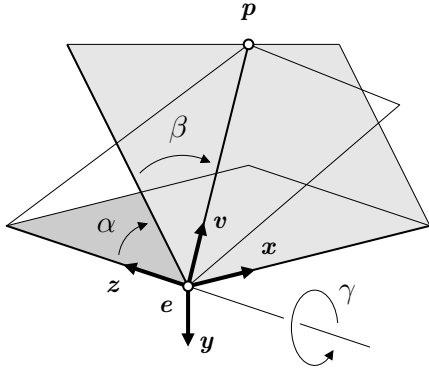


Fig. 6. Helmholtz Coordinates (c.f. fig. 3). The eye turns from the initial direction  $z$ , in order to fixate the point  $p$ , as in figure 3. This motion is represented as follows: The eye rotates through angle  $\beta$  around the axis  $y$ , after which the  $\{x, z\}$  plane is rotated by angle  $\alpha$  around axis  $x$ . In order to match the final Listing orientation, an initial cyclo-rotation around  $z$ , of angle  $\gamma$ , would be required.

$\mathbf{R}_H \mathbf{z}$ , while  $\{\mathbf{x}_H, \mathbf{y}_H\}$  are the rotated retinal axes.

The stereographic coordinates of the Helmholtz rotation are shown in figure 4b, where the bottom-to-top curves are parameterized by  $\alpha$ , and the left-to-right curves are parameterized by  $\beta$ . Furthermore, note that each side-to-side curve can be identified with the intersection of an epipolar plane with the viewing sphere. The orientations that result from the Helmholtz rotation scheme are illustrated in figure 5b. It is important to see that the crosses, by comparison with figure 5a, are no longer parallel. Rather, the ‘horizontal’ axis of each cross lies in the corresponding epipolar plane.

## VI. OCULAR TORSION

It has been shown in sections IV and V that the eye can be directed to a target  $p$  by a Listing rotation  $\mathbf{R}_L$ , or by a Helmholtz rotation  $\mathbf{R}_H$ ; hence

$$\mathbf{z}_L = \mathbf{z}_H = (v_x, v_y, v_z)^\top, \quad (16)$$

where  $v$  is the visual direction of  $p$ , as in (1). The Listing rotation accounts for the observed *orientation* of the eye, as well as for the direction. Hence, if Listing’s law is obeyed, then the vectors  $\mathbf{x}_L$  and  $\mathbf{y}_L$  are aligned with the horizontal and vertical meridians of the retina. However, the corresponding Helmholtz axes  $\mathbf{x}_H$  and  $\mathbf{y}_H$  are, in general, cyclo-rotated around the common direction  $v$ .

The discrepancy can be resolved by introducing a third rotation matrix, which represents the torsion around the primary direction  $z$ ;

$$\mathbf{C} = \begin{pmatrix} \cos \gamma & \sin \gamma & 0 \\ -\sin \gamma & \cos \gamma & 0 \\ 0 & 0 & 1 \end{pmatrix}. \quad (17)$$

Note that this cyclo-rotation is *anti-clockwise* from the subject’s point of view (i.e. looking out along the increasing  $z$  axis). For example, if  $\gamma = \pi/2$ , then  $\mathbf{C}\mathbf{y} = \mathbf{x}$ . This is consistent with the sense of  $\theta$ , which can be seen by comparison of figures 3 and 6.

The Listing rotation  $\mathbf{R}_L$  can now be represented in the Helmholtz system. The appropriate composition of (10) and (17) gives the equation

$$\mathbf{R}_L = \mathbf{ABC}. \quad (18)$$

The torsion angle  $\gamma$  in (17) that solves equation (18) must now be obtained in terms of the Euler angles  $\alpha$  and  $\beta$  in (11) and (12). This will be done in two steps; firstly the Listing meridian  $\mathbf{y}_L$  will be expressed in terms of  $\alpha$  and  $\beta$ . Secondly, the inclination of this meridian will be computed in the Helmholtz axes  $\mathbf{x}_H$  and  $\mathbf{y}_H$ .

It is straightforward to express  $\mathbf{y}_L$  in terms of the components of  $\mathbf{z}_L$ , by inspection of the second and third columns of the rotation matrix (7). The result, written in the notation of (16), is

$$\mathbf{y}_L = \begin{pmatrix} -v_x v_y, & \frac{1 + v_z - v_y^2}{1 + v_z}, & -v_y \end{pmatrix}^\top \quad (19)$$

where the fact that  $\sin^2 \phi = 1 - \cos^2 \phi = (1 + v_z)(1 - v_z)$  has been used. Equation (19) is the crux of the derivation because, using the equality (16), the components of  $v$  can be substituted from  $\mathbf{z}_H$ , which is defined in the *other* coordinate system (15). Now that both  $\mathbf{y}_L$  and  $\mathbf{y}_H$  are known in terms of  $(\alpha, \beta)$ , the cosine of the torsion angle is easily obtained;

$$\begin{aligned} \cos \gamma &= \mathbf{y}_L \cdot \mathbf{y}_H \\ &= \frac{\cos \alpha + \cos^2 \alpha \cos \beta + \sin^2 \alpha \cos \beta}{1 + v_z} \\ &= \frac{\cos \alpha + \cos \beta}{1 + \cos \alpha \cos \beta} \end{aligned} \quad (20)$$

where the identity  $\cos^2 \alpha + \sin^2 \alpha = 1$  has been used. This result is sufficient to define the torsion angle, as  $|\gamma| < \pi/2$ . However, it is also possible to compute the sine of the angle, as the dot product of  $\mathbf{y}_L$  with the reference axis  $\mathbf{x}_H$ . This is, by a derivation analogous to (20),

$$\begin{aligned} \sin \gamma &= \mathbf{y}_L \cdot \mathbf{x}_H \\ &= \frac{\sin \alpha \sin \beta}{1 + \cos \alpha \cos \beta}. \end{aligned} \quad (21)$$

The cosine (20) and sine equations (21) can be combined, to give the final result:

$$\tan \gamma = \frac{\sin \alpha \sin \beta}{\cos \alpha + \cos \beta}. \quad (22)$$

This equation can be put into a useful half-angle form, via the trigonometric identity  $\tan(\mu/2) = \tan \mu \sin \mu / (\tan \mu + \sin \mu)$ . With reference to (21) and (22), this gives

$$\tan \frac{\gamma}{2} = \tan \frac{\alpha}{2} \tan \frac{\beta}{2}. \quad (23)$$

The results (22) and (23) were originally obtained by Helmholtz [6], although the present derivation is different.

The meaning of the torsion formula (22) is illustrated in figure 7a. Here the location of each cross is determined by  $(\alpha, \beta)$ , as in figure 5b. However, in each direction  $(\alpha, \beta)$ , the eye has been cyclo-rotated by  $\gamma(\alpha, \beta)$ , in accordance with (22). The result is that the projected crosses are made mutually

parallel, as in the Listing figure 5a. Hence it can be seen that Listing’s law has been *simulated* in the Helmholtz coordinate system.

Equation (23) shows that the torsion  $\gamma$  will be zero if either  $\alpha$  or  $\beta$  is zero. These ‘secondary positions’ of the eye correspond to the parallel crosses on the horizontal and vertical meridians of figure 5b. If  $\alpha$  and  $\beta$  are both non-zero, then there are two qualitative cases. If  $\alpha$  and  $\beta$  have the same sign, then  $\gamma$  is positive, and the resulting cyclo-rotation is *anti-clockwise* from the subject’s point of view (17). These rotations map each cross in the upper-right and lower-left quadrants of figure 5b onto the corresponding cross in figure 7a. If  $\alpha$  and  $\beta$  have different signs, then  $\gamma$  is negative, and the rotation is *clockwise*. These rotations map each cross in the upper-left and lower-right quadrants of figure 5b onto the corresponding cross in figure 7a.

Consider, for example, the fixation of a distant scene-point in the upper mid-sagittal plane (i.e. ‘ahead’ and ‘up’), as in figure 1. This means that the elevation is  $\alpha > 0$ , while the left and right azimuths are  $\beta_\ell > 0$  and  $\beta_r < 0$ , respectively. Then it follows from (23) that, for each eye obeying Listing’s law, the *nasal* half of the horizontal retinal meridian will turn *up* out of the Helmholtz elevation plane (as in e.g. [31], [32]). Furthermore, a rotation (17) of the elevation plane by  $\gamma_\ell > 0$  around the left visual axis would align it with the horizontal meridian of the left retina. Likewise, a rotation (17) of the elevation plane by  $\gamma_r < 0$  around the right visual axis would align it with the horizontal meridian of the right retina.<sup>2</sup>

The preceding example of ‘ahead’ and ‘up’ fixation can also be described in relation to the *vertical* retinal meridians. In this case, the upper-halves of these meridians turn inwards (nasally) with respect to the head-fixed vertical direction.<sup>3</sup> This is commonly referred to as ‘intorsion’ of the vertical meridians [5].

It should be noted that equation (18) expresses the Listing rotation  $\mathbf{R}_L = \mathbf{ABC}$  in relation to head-fixed axes  $x$ ,  $y$  and  $z$ . It is straightforward to transform this to an eye-fixed representation  $\mathbf{R}_L = \mathbf{C}'\mathbf{B}'\mathbf{A}'$ . The matrices  $\mathbf{C}'$ ,  $\mathbf{B}'$  and  $\mathbf{A}'$  can be obtained from Rodrigues’ formula, with axes  $\mathbf{B}'\mathbf{A}'z$ ,  $\mathbf{A}'y$  and  $x$ , respectively.

## VII. APPROXIMATE MODELS

The Helmholtz torsion equation (22) is valid over the hemisphere of gaze angles  $\alpha, \beta \in [-90^\circ, 90^\circ]$ . The maximum range of human eye movements is smaller than this, and the typical range is much smaller; an average saccade magnitude of  $15^\circ$  has been reported [33]. This suggests that a simplified form of the torsion function (22) might be valid in practice. Moreover, there are three particular reasons to consider approximate torsion functions; firstly, a better understanding of the exact torsion function can be obtained. Secondly, the ease with which the visual system could represent the function  $\gamma(\alpha, \beta)$  is established. Thirdly, the approximations can be used to simplify the kinematics of the oculomotor system [3], [4].

<sup>2</sup>For comparison with the literature, these are the ‘Upper-nasal; Out’ cases in Westheimer’s tables I and II [12].

<sup>3</sup>Westheimer’s ‘Upper-nasal; In’ cases [12].

The Helmholtz torsion function (22), as noted in section VI, can be expressed in the half-angle form (23), with  $\tan(\gamma/2)$  on the left-hand side. Recall the truncated Taylor series  $\tan(\sigma) = \sigma + \sigma^3/3 + O(\sigma^5)$ . The half-angle version of this is therefore

$$\tan \frac{\sigma}{2} = \frac{\sigma}{2} + \frac{\sigma^3}{3 \times 2^3} + O(\sigma^5).$$

The corresponding series for  $\tan(\alpha/2)$  and  $\tan(\beta/2)$  are combined, according to (23). The following half-angle approximation is obtained, having discarded terms of total degree six (i.e.  $3 + 3$ ,  $1 + 5$ ,  $5 + 1$ ) and higher:

$$\tan \frac{\gamma}{2} \approx \frac{\alpha\beta}{4} + \frac{\alpha^3\beta}{48} + \frac{\alpha\beta^3}{48}. \quad (24)$$

Note that terms of total degree three and five are absent from the expansion of (23), owing to the saddle-like symmetries of the function.

The inverse-tangent can be approximated by the formula  $\tan^{-1}(\sigma\tau) = \sigma\tau + O(\sigma^3\tau^3)$ , where the total truncation degree matches that of (24). It follows that the second and fourth degree approximations of  $\gamma(\alpha, \beta)$  are

$$\gamma_2(\alpha, \beta) = \frac{\alpha\beta}{2} \quad (25)$$

$$\gamma_4(\alpha, \beta) = \frac{\alpha\beta}{2} + \frac{\alpha^3\beta}{24} + \frac{\alpha\beta^3}{24}. \quad (26)$$

The first of these (25) has appeared elsewhere (e.g. [4]). It can be seen that the approximations are much simpler than the original function (22); in particular, neither trigonometric nor inverse-trigonometric functions are involved.

The accuracy of the second-degree approximation (25) is visualized in figure 7b. If the approximation were perfect, then this plot would be identical to that in figure 7a. It can be seen that, inside the second ( $60^\circ$ ) circle, the two plots are visually indistinguishable. Differences in cyclo-rotation can, however, be clearly seen along the outer ( $90^\circ$ ) circle. The corresponding plot of the fourth-order (26) approximation is visually identical to that in figure 7a. A more formal evaluation will be made in the following section.

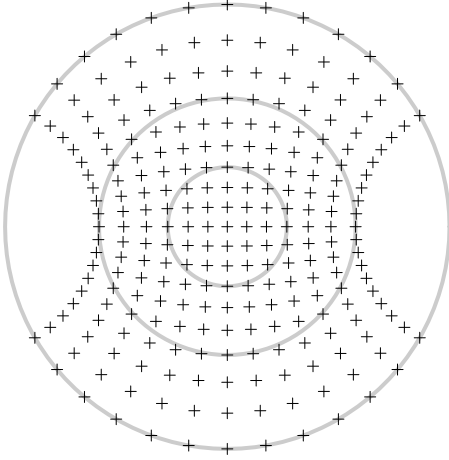
## VIII. NUMERICAL EVALUATION

The exact and approximate torsion functions will now be compared, over a range of visual directions. This will be done, intuitively, by moving the eye from primary position to a new direction, and evaluating the resulting torsion. This measurement will be averaged over a continuous range of visual directions. The range of directions will be defined by putting an upper limit on the eccentricity  $r$  of a visual target. Hence it is natural to choose a set of Listing directions, with  $0 \leq \phi \leq r$ , which can be converted to Helmholtz coordinates, for use in (25) and (26). The conversion is obtained by comparing the third columns of the matrices (7) and (15). If, as before, the eccentricity of the target is in the range  $0 \leq \phi \leq \pi/2$ , then

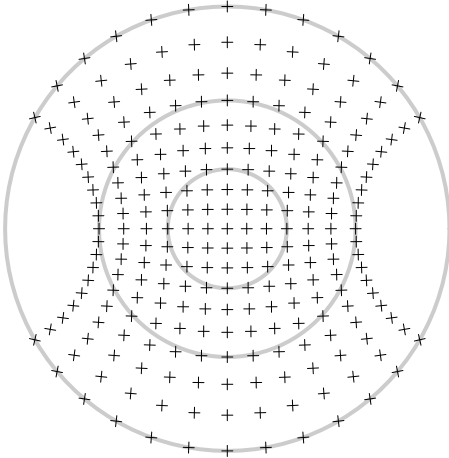
$$\alpha(\theta, \phi) = \tan^{-1} \frac{\sin \theta \sin \phi}{\cos \phi} \quad (27)$$

$$\beta(\theta, \phi) = \sin^{-1}(\cos \theta \sin \phi). \quad (28)$$





(a) Exact Listing Orientations, plotted in  $(\alpha, \beta)$  coordinates.



(b) Approximate Listing Orientations, plotted in  $(\alpha, \beta)$  coordinates.

Fig. 7. Listing orientations (7a), plotted in  $(\alpha, \beta)$  coordinates. Each orientation has been subject to a cyclo-rotation  $\gamma(\alpha, \beta)$ , resulting in mutually parallel stereographic crosses, as in fig. 5a. The *approximate* cyclo-rotation  $\gamma_2(\alpha, \beta)$ , defined in equation 25, has been used in (7b). The approximation is good for eccentricities of less than  $60^\circ$  (i.e. inside the second grey circle), but some tilting of the crosses can be seen in the periphery. See fig. 8 for a visualization of the difference between (7a) and (7b).

It is now straightforward to define a function  $\delta(\theta, \phi)$ , being the torsion value  $\gamma$ , measured in direction  $(\theta, \phi)$ ;

$$\delta(\theta, \phi) = \gamma(\alpha(\theta, \phi), \beta(\theta, \phi)). \quad (29)$$

The functions  $\delta_2(\theta, \phi)$  and  $\delta_4(\theta, \phi)$  are similarly defined from the approximations  $\gamma_2$  and  $\gamma_4$  respectively (25,26). The torsion error  $\epsilon_k(\theta, \phi)$ , will also be defined in Listing coordinates. This function measures the difference between the approximate and actual values,  $\delta_k$  and  $\delta$  respectively;

$$\epsilon_k(\theta, \phi) = \delta_k(\theta, \phi) - \delta(\theta, \phi). \quad (30)$$

The accuracy of the  $k$ -th order approximation can be evaluated by integrating a suitable function of  $\epsilon_k$  over a region of visual directions  $(\theta, \phi)$ . Such integrals could be studied analytically, but a numerical approach will be preferred here. This choice

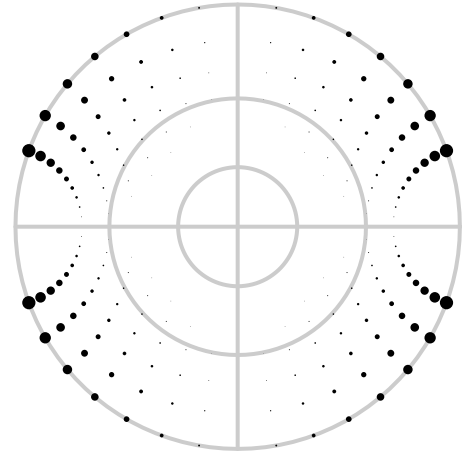


Fig. 8. Visualization of the difference between the actual torsion (7a) and the  $\gamma_2$  approximation (7b), plotted in  $(\alpha, \beta)$  coordinates. Larger discs represent worse approximations, as can be confirmed by comparing figs. (7a) and (7b). Note that the large errors occur in directions that have high absolute elevation  $|\alpha|$  and high absolute azimuth  $|\beta|$ . Errors of less than  $0.5^\circ$  are not shown; otherwise the disc radii are proportional to  $|\gamma_2(\alpha, \beta) - \gamma(\alpha, \beta)|$ . The horizontal and vertical meridians shown in grey, for reference.

allows the integrand, and the region of integration, to be chosen with more freedom. In particular, the absolute value of the error can be integrated.

The notation  $|g|_0^r$  represents the functional that returns the average absolute value of a function  $g(\theta, \phi)$ , computed over a range of visual directions  $0 \leq \theta \leq 2\pi$  and  $0 \leq \phi \leq r$ . This is defined as

$$|g|_0^r = \frac{1}{A(r)} \int_0^{2\pi} \int_0^r \sin(\phi) |g(\theta, \phi)| d\phi d\theta \quad (31)$$

where  $\sin(\phi)$  is the scalar Jacobian. The normalization term  $A(r)$  is the area of the spherical cap, over which the integration is performed. This term is easily obtained from the formula

$$A(r) = 2\pi(1 - \cos r). \quad (32)$$

The integral (31) was evaluated by a standard numerical routine [34]. Table I shows the results of the evaluation. Each functional  $|g|_0^r$  was evaluated for all eye-movements up to eccentricity  $r = 15^\circ, 30^\circ, 45^\circ, 60^\circ, 75^\circ$ . Note that  $0 \leq \phi \leq 30^\circ$  represents a ‘typical’ range of human eye movements, while  $0 \leq \phi \leq 60^\circ$  extends to the maximum physical range. The upper limit can be reached, by humans, in the downward direction. The first row of the table gives the mean absolute torsion  $|\delta|_0^r$ , evaluated in the Helmholtz system. These values, which do not seem to have been computed previously, are useful for gauging the significance of the approximation errors. The second and third rows of the table give the average errors  $\epsilon_2$  and  $\epsilon_4$  that are associated with torsion approximations  $\gamma_2$  and  $\gamma_4$ , respectively (25,26). Hence the relative error of the approximations can be computed from  $|\epsilon_k|_0^r / |\delta|_0^r$ .

The principal conclusion is that the second-order approximation  $\gamma_2(\alpha, \beta) = \frac{1}{2}\alpha\beta$  has an average error of  $0.02^\circ$  for  $\phi \leq 30^\circ$ , and of  $0.4^\circ$  for  $\phi \leq 60^\circ$ . As fractions of the average torsion  $|\delta|_0^r$ , these numbers represent errors of 1.6% and 7.3%,

TABLE I  
ABSOLUTE VALUES OF THE ACTUAL TORSION  $\delta(\theta, \phi)$ , AND  
APPROXIMATION ERROR  $\epsilon_k(\theta, \phi)$ , AVERAGED OVER INCREASINGLY  
LARGE REGIONS OF THE VIEWING SPHERE.

	$r = 15^\circ$	$r = 30^\circ$	$r = 45^\circ$	$r = 60^\circ$	$r = 75^\circ$
$ \delta _0^r$	0.314°	1.280°	2.978°	5.596°	9.630°
$ \epsilon_2 _0^r$	0.001°	<b>0.020°</b>	<b>0.112°</b>	<b>0.407°</b>	1.271°
$ \epsilon_4 _0^r$	$1.45^\circ \times 10^{-5}$	0.001°	0.011°	0.075°	0.396°

respectively. Hence for typical eye movements ( $\phi \leq 30^\circ$ ) the second order approximation is adequate, given that eye-movements can typically be measured to a precision of around one degree [5]. The table also shows that, for all achievable eye movements ( $\phi \leq 60^\circ$ ), the fourth-order model  $\gamma_4$  is adequate.

### IX. SYNTHETIC TORSION

It will now be shown that the results obtained in sections IV–VII can be used to *synthesize* the effect of Listing’s law on images that have been obtained from a pan-tilt camera mounting. Moreover, this will be done in a way that is physically consistent with the original camera. This means that the synthetic image will match the one that would have been obtained after the corresponding cyclo-rotation of the camera. It is important to ensure physical consistency, so that subsequent algorithms need not distinguish between the original and the synthetic images. This cannot, in general, be achieved simply by rotating the original images around their centre-points. The appropriate image transformation must be defined in relation to the projection matrix of the camera, as shown below. Note that it will usually be more convenient, and faster, to extract features (e.g. points or edges) in the *original* image, and then to transform the coordinates of the features. This avoids the need to resample or crop the pixel-data.

It will be assumed that the camera and ocular projections can be approximated by the usual pin-hole model [1]. Furthermore, it will be assumed that the nodal points of the optics coincide at the fixed rotational centre  $e = (0, 0, 0)^\top$  of the camera, as in (2). Each scene point  $\mathbf{q}$  has coordinates  $(x, y, z)^\top$ , as described in section II. The perspective projection is obtained via the  $3 \times 3$  matrix  $\mathbf{M}$ , resulting in homogeneous ‘eye-coordinates’  $\mathbf{q}_E = (x_E, y_E, z_E)^\top$ , with corresponding pixel-positions  $(x_E/z_E, y_E/z_E)^\top$ . This means, with reference to (2), that

$$\mathbf{q}_E = \mathbf{M}\mathbf{q} \quad (33)$$

$$= \mathbf{S}\mathbf{R}^\top\mathbf{q} \quad (34)$$

where  $\mathbf{R}^\top$  is the scene-to-eye rotation, and  $\mathbf{S}$  performs an affine transformation of the image, to account for the ‘intrinsic’ parameters of the camera (as described below). Note that the rotation is transposed, for consistency with (2). In particular, it follows from (1) and (2) that the projection of the fixated point  $\mathbf{p}$  is  $\mathbf{S}\mathbf{z}$ . For a perfect pan-tilt mounting, the rotation  $\mathbf{R}^\top$  would have the form  $\mathbf{B}^\top\mathbf{A}^\top$ , based on definitions (11) and (12). In practice, the camera matrix  $\mathbf{M}$  (as in 33) can be estimated by standard methods, and decomposed as follows

[1]. The matrices  $\mathbf{S}$  and  $\mathbf{R}^\top$  (as in 34) are obtained by  $RQ$ -factorization<sup>4</sup> of  $\mathbf{M}$ . The first factor can be written as

$$\mathbf{S} = \begin{pmatrix} s_{11} & s_{12} & x_0 \\ 0 & s_{22} & y_0 \\ 0 & 0 & 1 \end{pmatrix}. \quad (35)$$

This matrix contains the pixel-coordinates  $(x_0, y_0)^\top$  of the principal point (intersection of the optical axis with the image plane), two scale-factors  $(s_{11}, s_{22})$ , and a parameter  $s_{12} \approx 0$  which allows for a skew between the horizontal and vertical axes of the sensor. In more detail,  $s_{11} = fg_x$  and  $s_{22} = fg_y$ , where  $f$  is the focal-distance of the camera, and the scales  $(g_x, g_y)$  determine the number of pixels per unit distance in the horizontal and vertical dimensions.

These intrinsic parameters (35) should not be changed by a synthetic cyclo-rotation  $\mathbf{C}^\top$  of the image. Note, however, that the naive procedure  $\mathbf{C}^\top\mathbf{q}_E$  would imply a camera  $\mathbf{C}^\top\mathbf{S}\mathbf{R}^\top$ , according to the projection model (34). The matrices  $\mathbf{C}^\top$  and  $\mathbf{S}$  do not, in general, commute. It follows that  $\mathbf{S}$  would not be recovered from the  $RQ$ -factorization of the implied camera (owing to the uniqueness of the factorization). For this reason, the cyclo-rotated points are properly defined as

$$\mathbf{q}'_E = \mathbf{S}\mathbf{C}^\top\mathbf{S}^{-1}\mathbf{q}_E. \quad (36)$$

This definition, with reference to (34), implies the existence of a synthetic camera matrix

$$\begin{aligned} \mathbf{M}' &= \mathbf{S}\mathbf{C}^\top\mathbf{S}^{-1}\mathbf{M} \\ &= \mathbf{S}\mathbf{C}^\top\mathbf{R}^\top \end{aligned}$$

It is clear from (34) that the matrix  $\mathbf{M}'$  has the  $RQ$ -factorization  $\mathbf{S} \cdot \mathbf{C}^\top\mathbf{B}^\top\mathbf{A}^\top$ , and is therefore consistent with the original set of intrinsic parameters (35). In practice, it may be more convenient to work with ‘normalized coordinates’  $\mathbf{S}^{-1}\mathbf{q}_E$ , where the effects of the intrinsic parameters have been undone. In this case, the cyclo-rotated *and* normalized coordinates are simply

$$\mathbf{q}''_E = \mathbf{C}^\top\mathbf{S}^{-1}\mathbf{q}_E \quad (37)$$

The product  $\mathbf{C}^\top\mathbf{S}^{-1}$  can be formed first, so that a single affine transformation is applied to the observed feature-coordinates  $\mathbf{q}_E$ . Note that this is a 2-D transformation, depending only on the intrinsic parameters (35) and the cyclo-rotation angle  $\gamma$ . In the special case that the upper-left  $2 \times 2$  block of  $\mathbf{S}$  is a multiple  $s\mathbf{I}_2$  of the identity matrix, the procedure (37) simply translates the principal point  $(x_0, y_0)^\top$  to  $(0, 0)^\top$ , before scaling and rotating the feature-coordinates by  $s$  and  $\gamma$ , respectively. In general, however,  $s_{11} \neq s_{22}$  and  $s_{12} \neq 0$ , meaning that the transformation (37) should be used.

If the cyclo-rotation angle  $\gamma$  is defined by (22), then the new coordinates  $\mathbf{q}''_E$  (as well as the  $Q$  factor of the implied camera matrix) are subject to Listing’s law, as well being physically consistent with the original camera. Other aspects of biological vision, such as the non-uniform distribution of photoreceptors on the retina [35], can be modelled by further

<sup>4</sup>The decomposition  $\mathbf{M} = \mathbf{R}\mathbf{Q}$  has an upper-triangular factor  $\mathbf{R}$ , and an orthogonal factor  $\mathbf{Q}$ . The decomposition is unique if, as here,  $\mathbf{M}$  has full-rank, and  $\mathbf{R}$  is required to have positive elements on the diagonal.

transformations of the new coordinates. It is also possible to adapt the above model to a spherical projection, which may be more appropriate for the human eye; in this case the observed feature-coordinates are  $(x_E/d, y_E/d)^\top$ , where  $d = |\mathbf{q}|$  is the distance to the point, as in (1).

## X. DISCUSSION

It has been shown in sections II–VI that Listing’s law can be formulated in terms of rotation matrices. This means that the usual computer vision camera-model (34) can easily be adapted to the human eye, as shown in section IX. Two polynomial approximations of the torsion function  $\gamma(\alpha, \beta)$  were derived in section VII. A procedure for numerical integration over visual directions was introduced in section VIII. The average cyclo-rotation was computed, and the two approximations were validated. Finally, in section IX, it was shown that Listing’s law can be *imposed* on a suitable set of calibrated images.

There is considerable interest in the relationship between Listing’s law and other visual processes, such as stereopsis [2], [4]. For example; if the binocular fixation point is relatively close, then Listing’s law must be modified [36], [37]. Future work will include an extension of the present analysis to the binocular case [15]. The results presented here, as described in the introduction, make it possible to evaluate such models with respect to real images.

The implications of section VII, with regard to the neural representation of eye-movements, are also interesting. It is clear that the cyclo-rotation angle is a slowly-varying function of visual direction, over the typical range of eye movements. Indeed, the results of section VIII show that the observed cyclo-rotation is effectively proportional the product of the eye’s azimuth and elevation. This suggests that Listing’s law could be represented quite directly in the primate oculomotor system [3].

## REFERENCES

- [1] R. Hartley and A. Zisserman, *Multiple View Geometry in Computer Vision*. Cambridge University Press, 2000.
- [2] J. J. Koenderink and A. van Doorn, “Geometry of Binocular Vision and a Model for Stereopsis,” *Biological Cybernetics*, vol. 21, pp. 29–35, 1976.
- [3] A. V. van den Berg, “Kinematics of Eye Movement Control,” *Proc. R. Soc. Lond. B*, vol. 260 (1358), pp. 191–197, 1995.
- [4] D. Tweed, “Visual-Motor Optimization in Binocular Control,” *Vision Research*, vol. 37(14), pp. 1939–1951, 1997.
- [5] R. H. S. Carpenter, *Movements of the Eyes*. Pion, 1988.
- [6] H. L. F. von Helmholtz, *Treatise on Physiological Optics, Vol. III (3rd ed., trans. J. P. C. Southall)*. Optical Society of America, 1925.
- [7] D. Tweed and T. Vilis, “Geometric Relations of Eye Position and Velocity Vectors during Saccades,” *Vision Research*, vol. 30(1), pp. 111–127, 1990.
- [8] D. Tweed, W. Cadera, and T. Vilis, “Computing Three-Dimensional Eye Position Quaternions and Eye Velocity from Search Coil Signals,” *Vision Research*, vol. 30(1), pp. 97–110, 1990.
- [9] P. S. Sandor, M. A. Frens, and V. Henn, “Chameleon Eye-Position obeys Listing’s Law,” *Vision Research*, vol. 41, pp. 2245–2251, 2001.
- [10] W. Zhu and W. M. King, “Binocular Eye Movements Not Coordinated during REM Sleep,” *Experimental Brain Research*, vol. 117, pp. 153–160, 1997.
- [11] K. Hepp, “Theoretical Explanations of Listing’s Law and their Implications for Binocular Vision,” *Vision Research*, vol. 35(23–24), pp. 3237–3241, 1995.
- [12] G. Westheimer, “Kinematics of the Eye,” *Journal of the Optical Society of America*, vol. 47(10), pp. 967–974, 1957.
- [13] D. A. Robinson, “A Quantitative Analysis of Extraocular Muscle Cooperation and Squint,” *Investigative Ophthalmology*, pp. 801–825, November 1975.
- [14] T. Haslwanter, “Mathematics of Three-Dimensional Eye-Rotations,” *Vision Research*, vol. 35(12), pp. 1727–1739, 1995.
- [15] M. Hansard and R. Horaud, “Cyclopean Geometry of Binocular Vision,” *Journal of the Optical Society of America A*, vol. 25(9), pp. 2357–2369, 2008.
- [16] O. Bolina and L. H. A. Monteiro, “Kinematics of Eye Movement,” *Ophthalmic & Physiological Optics*, vol. 20(1), pp. 59–62, 2000.
- [17] D. W. Murray, F. Du, P. F. McLauchlan, I. D. Reid, P. M. Sharkey, and M. Brady, “Design of Stereo Heads,” in *Active Vision*, A. Blake and A. Yuille, Eds. MIT Press, 1992.
- [18] J. P. Barreto and H. Araujo, “General Framework for Selecting World Coordinate Systems in Perspective and Catadioptric Imaging Applications,” *International Journal of Computer Vision*, vol. 57(1), pp. 23–47, 2004.
- [19] M. R. M. Jenkin and J. K. Tsotsos, “Active Stereo Vision and Cyclo-torsion,” in *Proc. IEEE CVPR*, 1994, pp. 806–811.
- [20] G. Cannata and M. Maggiali, “Models for the Design of Bioinspired Robot Eyes,” *IEEE Trans. Robotics*, vol. 24(1), pp. 27–44, 2008.
- [21] D. A. Robinson, “The Oculomotor Control System: A Review,” *Proc. IEEE*, vol. 56(6), pp. 1032–1049, 1968.
- [22] L. R. Young and D. Sheena, “Survey of Eye Movement Recording Methods,” *Behavior Research Methods and Instrumentation*, vol. 7(5), pp. 397–439, 1975.
- [23] K. R. Park, “A Real-Time Gaze Position Estimation Method Based on a 3-D Eye-Model,” *IEEE Trans. Syst., Man, Cybern. B*, vol. 37(1), pp. 199–212, 2007.
- [24] A. Villanueva and R. Cabeza, “A Novel Gaze Estimation System with One Calibration Point,” *IEEE Trans. Syst., Man, Cybern. B*, vol. 38(4), pp. 1123–1212, 2008.
- [25] T. Haslwanter and S. T. Moore, “A Theoretical Analysis of Three-Dimensional Eye Position Measurement Using Polar Cross-Correlation,” *IEEE Trans. Bio-Med. Eng.*, vol. 42(11), pp. 1053–1061, 1995.
- [26] J. Stuelpnagel, “On the Parametrization of the Three-Dimensional Rotation Group,” *SIAM Review*, vol. 6(4), pp. 422–430, 1964.
- [27] W. Hausteiner, “Considerations on Listing’s Law and the Primary Position by Means of a Matrix Description of Eye Position Control,” *Biological Cybernetics*, vol. 60, pp. 411–420, 1989.
- [28] K. Hepp, “On Listing’s Law,” *Communications in Mathematical Physics*, vol. 132, pp. 285–292, 1990.
- [29] D. Hestenes, “Invariant Body Kinematics: I. Saccadic and Compensatory Eye Movements,” *Neural Networks*, vol. 7, pp. 65–77, 1994.
- [30] S. Judge, “Reflection Makes Sense of Rotation of the Eyes,” *Vision Research*, vol. 46, pp. 3862–3866, 2006.
- [31] R. A. B. Somani, J. F. X. Desouza, D. Tweed, and T. Vilis, “Visual Test of Listing’s Law during Vergence,” *Vision Research*, vol. 38(6), pp. 911–923, 1997.
- [32] I. T. C. Hooge and A. V. van den Berg, “Visually Evoked Cyclovergence and Extended Listing’s Law,” *J. Neurophysiol.*, vol. 83, pp. 2757–2775, 2000.
- [33] A. T. Bahill, D. Adler, and L. Stark, “Most Naturally Occurring Human Saccades have Magnitude of 15 degrees or less,” *Investigative Ophthalmology*, vol. 14, pp. 468–469, 1975.
- [34] A. Genz and A. A. Malik, “An Adaptive Algorithm for Numerical Integration over an  $N$ -Dimensional Rectangular Region,” *J. Comp. Appl. Math.*, vol. 6, pp. 295–302, 1980.
- [35] C. A. Curcio, K. R. Sloan, R. E. Kalina, and A. E. Hendrickson, “Human Photoreceptor Topography,” *J. Comparative Neurology*, vol. 292, pp. 497–523, 1990.
- [36] D. Mok, A. Ro, W. Cadera, J. D. Crawford, and T. Vilis, “Rotation of Listing’s Plane during Vergence,” *Vision Research*, vol. 32(11), pp. 2055–2064, 1992.
- [37] L. J. van Rijn and A. V. van den Berg, “Binocular Eye Orientation during Fixation: Listing’s Law extended to include Eye Vergence,” *Vision Research*, vol. 33, pp. 691–708, 1993.

**Miles Hansard** is a post-doctoral researcher at INRIA Rhône-Alpes, France. He is interested in geometric and computational aspects of visual perception. His recent work is concerned with human and robotic stereopsis. He studied Experimental Psychology (BSc) and Computer Vision (MRes, PhD) at University College London.

**Radu Horaud** holds a position of director of research at INRIA Rhône-Alpes, France. His research interests cover computer vision, machine learning, multi-sensory fusion, and robotics. He is the author of over 100 scientific publications. He is an area editor of *Computer Vision and Image Understanding* (Elsevier), a member of the advisory board of *The International Journal of Robotics Research* (Sage), and a member of the editorial boards of *The International Journal of Computer Vision* (Kluwer), *Image and Vision Computing*, and *Machine Vision and Applications* (Springer). In 2001 he served as program co-chair of the IEEE Eighth International Conference on Computer Vision (ICCV'01).